Dennis Wiedemann, Andreas Grohmann

3d-and 4d-metal(II) complexes of a tris(pyridyl)ethane-derived N-4 ligand – a structural study and reactivity remarks

This is the peer reviewed version of the following article:

Wiedemann, Dennis; Grohmann, Andreas: 3d-and 4d-metal(II) complexes of a tris(pyridyl)ethane-derived N-4 ligand – a structural study and reactivity remarks. - Zeitschrift für anorganische und allgemeine Chemie. - ISSN: 1521-3749 (online), 0044-2313 (print). - 640 (2014), 8–9 - pp. 1632–1640. - DOI: 10.1002/zaac.201400047. *(Postprint version is cited, page numbers differ.)*

which has been published in final form at https://dx.doi.org/10.1002/zaac.201400047. This article may be used for non-commercial purposes in accordance with Wiley Terms and Conditions for Self-Archiving.

ARTICLE

DOI: 10.1002/zaac.201400047

3d- and 4d-Metal(II) Complexes of a Tris(pyridyl)ethane-Derived N_4 Ligand—A Structural Study and Reactivity Remarks

Dennis Wiedemann[a] and Andreas Grohmann*[a]

Keywords: N ligands; Coordinative strain; Tetradentate ligands; 3d-Metal complexes; X-ray structure analysis

Abstract. A series of complexes of the new N_4 chelate ligand L (L = 1-{6-[1,1-di(pyridin-2-yl)ethyl]pyridin-2-yl}-*N*,*N*-dimethylmethanamine) with intermediate to late divalent transition metal ions M has been obtained by the reaction between L and the respective chloride salt or similar precursor in methanol: $[MCl_2L]$ (M = Mn, Fe, Co, Ni, Zn; Ru) and [CuClL]Cl. The stereochemical characteristics of the chelate ligand were studied by means of single-crystal X-ray diffraction, and quantified on the basis of several geometric parameters, including the tetragonal distortion Σ and the continuous symmetry measure $S(O_h)$. The overall distortion of the coordination environment is predominantly determined by the steric demand of the central ion, while electronic or other subtler influences essentially contribute to the distortion of the ligand L. Unlike similar complexes, $[Mn^{II}Cl_2L]$ cannot be oxidised to a manganese(III) complex by dioxygen, hydrogen peroxide or iodosylbenzene. In $[Ru^{II}Cl_2L]$, one chlorido ligand can be exchanged against small π-accepting molecules such as acetonitrile or dinitrogen. L offers an environment ideal for small metal ions (0.4–0.6 Å), such as low-spin iron(II), which rationalises the late onset of thermal spin crossover in the complex $[Fe^{II}L(NCS)_2]$.

* Prof. Dr. A. Grohmann
Fax: +49 30 314-22935
E-Mail: andreas.grohmann@chem.tu-berlin.de
[a] Institut für Chemie
Technische Universität Berlin
Straße des 17. Juni 135
10623 Berlin, Germany

Introduction

Chelating N ligands have been used extensively in coordination chemistry and related fields, such as bioinorganic chemistry, metal-organic chemistry, supramolecular chemistry, materials chemistry, and homogeneous catalysis.[1] We are interested in ligands having a podand topology and mixed imine/amine donor sets, where the variation of the ratio of donor atoms (imine vs. amine) allows us to tune the electronic character ("electron poor" vs. "electron rich") of the central ion, depending on the relative numbers of π-accepting (imine) vs. σ-donating (amine) donors. A series of such N_5 ligands, which leave a single "labile" coordination site in octahedral complexes, have provided iron(II) coordination modules showing particularly diverse redox chemistry, including nitrite reductase reactivity.[2]

A logical extension of this chemistry is to N_4 ligand caps which, in octahedral complexes, leave two *cis*-positioned coordination sites for small monodentate ligands. The ligand 1-{6-[1,1-di(pyridin-2-yl)ethyl]pyridin-2-yl}-*N*,*N*-dimethylmethanamine (L, see Fig. 1) has already proven its versatility, in that it forms unusual iron(II) and copper(I) complexes. It is readily prepared from 2-ethylpyridine, 2-fluoropyridine and 2,6-dibromopyridine in a sequence of twofold nucleophilic aromatic substitution, cyanation, hydrogenation and *Eschweiler-Clarke* dimethylation.[3] Complexes are then conveniently synthesised by addition of metal salts, with or without subsequent exchange of the monodentate ligands, as required.

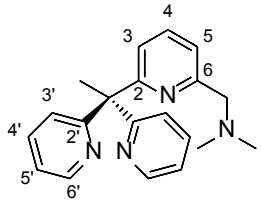

Figure 1. Structural formula of the mixed amine-pyridine ligand L used in this study, with atom numbering scheme.

This procedure has provided the compound $[Cu^{I}L(MeCN)]PF_6$ (**5b**), which shows an unusual anaerobic oxidation chemistry and potentially mimics peptidylglycine α-hydroxylating monooxygenase (PHM) or copper-containing amine-oxidase reactivity. The ferrous complex $[Fe^{II}(CN)_2L]$ (**2c**) is a photosensitiser, and enables photoelectrochemical photocurrent switching (PEPS) when adsorbed on titanium-dioxide surfaces.[3b] The bis(thiocyanato) complex $[Fe^{II}L(NCS)_2]$ (**2d**), when deposited as a submonolayer on graphite, undergoes thermally induced, fully reversible, gradual one-step spin-crossover (SCO) without hysteresis; it is one of very few compounds known to date, which are capable of such transitions in direct contact with a surface.[4] The SCO correlates with structural features in solutions, powders and crystals of **2d**, and comparison with the complexes $[Fe^{II}Cl_2L]$ (**2a**) and $[Fe^{III}Cl_2L]PF_6$ (**2b**) elucidated further details.[5] Why the transition temperature in **2d** is relatively high has, however, remained an open question; also, the coordination chemistry of this ligand with other transition metal ions has been largely unexplored.

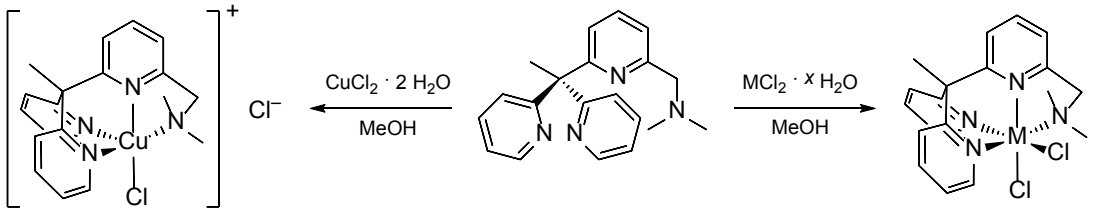

Scheme 1. Synthesis of complexes **1**–**6** (M: 3d-metal, *x*: hydration number).

In this contribution, we present structures and properties of the compounds [$M^{II}Cl_2L$] (M: Mn [**1**], Co [**3**], Ni [**4**], Zn [**6**]) and [$Cu^{II}ClL$]Cl (**5a**), thus completing a series with central to late 3d-metals and addressing the questions mentioned above. In addition, the full characterisation of the ruthenium complexes [$Ru^{II}Cl_2L$] (**7a**) and [$Ru^{II}ClL(MeCN)$]I (**7b**) illustrates the possibility to synthesise 4d-metal complexes.

Results and Discussion

Synthesis of 3d-Metal Complexes

The dichloridometal(II) complexes **1**–**6** (manganese to zinc) are readily synthesised via addition of L to the corresponding metal(II) chloride (hydrate) in methanol (see Scheme 1). Precipitation with methyl-*tert*-butyl ether (MTBE) yields the desired compounds—in most cases as well defined solvates—in medium to high yields. Bromido analogues may be prepared in the same way, as checked for iron(II), copper(II) and zinc(II).

Crystal-Structure Analyses

The electroneutral complexes **1**–**4** and **6** crystallise in the monoclinic space group $P2_1/c$; the cationic complex **5a** crystallises in the centred (monoclinic) space group $C2/c$. (The analogous bromido compounds mentioned above crystallise in the monoclinic system with cell parameters very similar to those of the chlorido complexes. Their crystals are either isotypic, or *C* centred if solvent is absent.) Molecules are depicted in Fig. 2, crystallographic data and structure refinement details summarised in Table 1.

Except for copper(II) in **5a**, all metal(II) ions are coordinated in a distorted octahedral fashion. The respective bond lengths vary within a range typical for the substance class (see Table 2). Due to constraints imposed by the rigidity of L and the strong Jahn-Teller effect expected for d^9 systems, the copper(II) ion in **5a** is coordinated by only five donors. The sixth possible donor (Cl2) is at a non-bonding distance, making N30–Cu1···Cl2 the axis of distortion. N10 of the pyridinediyl residue is a slightly weaker donor than the pyridyl N-atoms (cf. selective protonation of N20, N30 and N41 in L · 3 HBr).[3b] As a result of a *trans* influence, the bond to Cl2—diametrically opposite the stronger donor N20—is weakened, which makes this axis the preferred direction of elongation. The coordination polyhedron around copper(II) is intermediate between a trigonal bipyramid and a square pyramid. However, the analysis of continuous symmetry measures (CSM), quantifying "the minimal distance movement that the points of an object have to undergo in order to be transformed into a shape of the desired symmetry",[6] shows the latter to be the more appropriate description ($S[C_{4v}] = 2.96$ as opposed to $S[D_{3h}] = 4.54$).

Intermolecular interactions are similar among the different compounds: CH···Cl contacts occur in all of them; methanol molecules—if present—donate hydrogen bonds to Cl2. In the case of [$Cu^{II}ClL$]Cl (**5a**), these are the chloride counterions forming layers in (100). Except for [$Ni^{II}Cl_2L$] (**4**), all complexes form π stacks with their neighbours (one per molecule in **1**, **2a**, **3** and **6**, two in **5a**).

Table 2. Coordinative bond lengths *d*/Å in 3d-metal(II) complexes.

	[$MnCl_2L$] (**1**)	[$FeCl_2L$] (**2a**)[a]	[$CoCl_2L$] (**3**)	[$NiCl_2L$] (**4**)	[$CuClL$]Cl (**5a**)	[$ZnCl_2L$] (**6**)
M1–N10	2.2543(17)	2.1710(18)	2.101(2)	2.0395(17)	1.971(3)	2.156(2)
M1–N20	2.2659(17)	2.1935(19)	2.124(2)	2.0746(16)	2.049(3)	2.152(2)
M1–N30	2.3806(16)	2.226(2)	2.196(2)	2.1472(16)	2.275(3)	2.294(2)
M1–N41	2.3262(17)	2.2913(19)	2.261(2)	2.2084(16)	2.072(3)	2.274(2)
M1–Cl1	2.4093(6)	2.3455(6)	2.3588(8)	2.3879(6)	2.2309(9)	2.3221(7)
M1–Cl2	2.4674(6)	2.5570(7)	2.4784(9)	2.4634(5)	3.397(1)[b]	2.4702(8)

[a] Data have been published before and are included for comparison.[3b, 5] [b] Non-bonded distance.

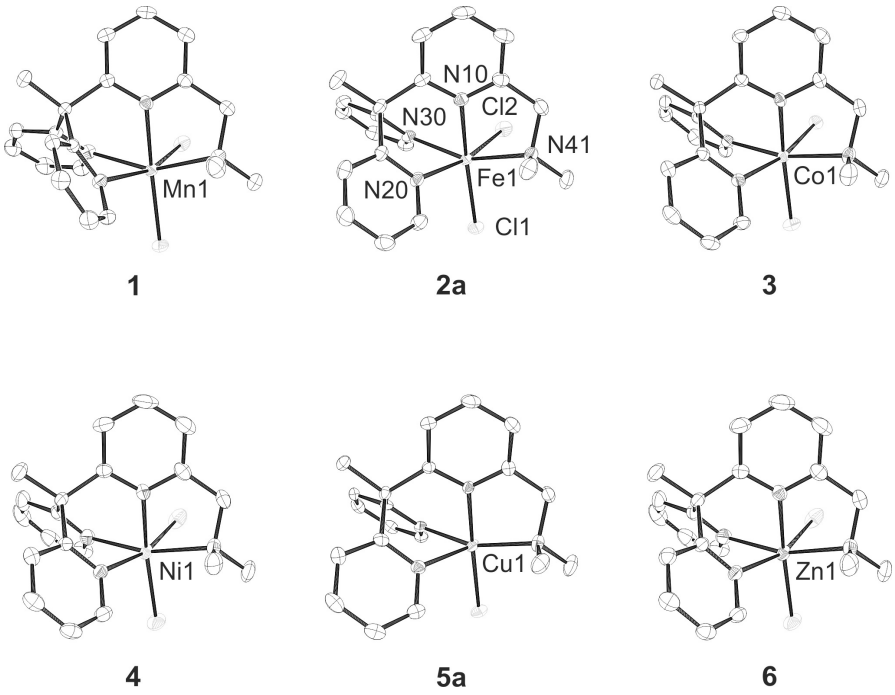

Figure 2. ORTEP plots of the 3d-metal(II) complexes of L. Ellipsoids for 50 % probability, hydrogen atoms, solvent molecules and chloride counter-ion of **5a** omitted for clarity.

Effects of the Metal-Ion Size

Optical inspection of the molecular structures reveals differing degrees of distortion in the coordination polyhedra and ligand geometries. Further examination of coordinative and intra-ligand angles corroborates this finding. In order to quantify distortion and correlate it with steric or electronic influences, we evaluated well-established measures of distortion for the coordination environment:

- the displacement Δr of the central ion from the centre of the coordination octahedron,
- the tetragonal distortion Σ, being the sum of the deviations of all twelve *cis* angles in the octahedron from 90°,[7] and
- the continuous symmetry measure (CSM) $S(O_h)$ for the overall deviation from an isometric octahedron.

While Δr is insensitive towards centre-point invariant (e.g., inversion symmetric) distortion and Σ is insensitive towards changes in bond lengths, $S(O_h)$ covers all deviations from ideal symmetry. It may adopt values between 0 (full symmetry) and 100 (lowest possible agreement). For an ideal octahedron, $\Delta r = \Sigma = S(O_h) = 0$. As there are no common measures for distortion in complex polydentate ligands, we defined two parameters in analogy to Σ (see Fig. 3), describing features that are particularly striking.

The ring tilt Ξ is the sum of the deviations of the three individual ring-tilt angles ξ_n from 180° (see Eq. 1). Each of these is an angle between one ring centroid R*n* and the nitrogen-metal bond (N*n*0–M1).

$$\Xi = \sum_{n=1}^{3} \left| \xi_n - 180° \right| \quad \text{with} \quad \xi_n = \angle(\text{R}n\text{–N}n0\text{–M1}) \tag{1}$$

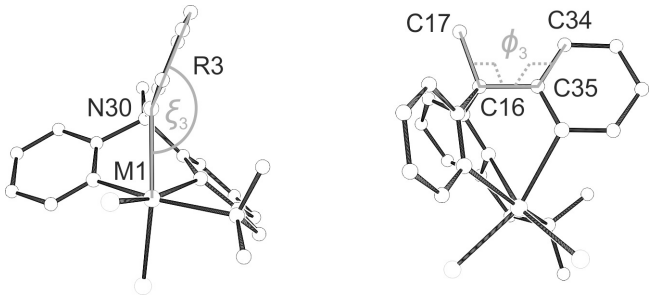

Figure 3. Definition of the individual ring-tilt angles ξ_n (left) and ring-twist angles ϕ_n (right) for the example of $n = 3$ in complex **1** (see also text; atoms with arbitrary radii, hydrogen atoms omitted for clarity).

The ring twist Φ, on the other hand, is the sum of the deviations of the three individual ring-twist angles ϕ_n from 0° (see Eq. 2). These are the torsion angles between the "central" methyl carbon–quaternary-carbon bond (C16–C17) and a representative adjacent ring-bond (C*n*4–C*n*5).

$$\Phi = \sum_{n=1}^{3} \left| \phi_n \right| \quad \text{with} \quad \phi_n = \angle(\text{C}n4\text{–C}n5\text{–C16–C17}) \tag{2}$$

Ideally, the σ-donating and π-accepting pyridine rings would coordinate with $\Xi = \Phi = 0$, making the substituted tris(pyridyl)ethane cap fit accurately without any strain or distortion. The steric demand of the central ion is adequately quantified by its effective ionic radius r_{eff},[8] which depends on coordination number, type of polyhedron and spin state. The latter has been verified by means of susceptometry at room temperature (see Table 3). The effective magnetic moments μ_{eff} fall in ranges typical for the central ions.[9] As was anticipated for weak-field halogenido ligands, chlorido complexes of $3d^4$- to $3d^7$-metals adopt a high-spin (HS)

configuration. An SCO at lower temperature—than used for crystal-structure determination—is very unlikely for these complexes and would be unprecedented. In $[Fe^{II}(CN)_2L]$ (**2c**), the strong-field cyanido-ligand leads to a low-spin (LS) configuration, whereas in $[Ru^{II}Cl_2L]$ (**7a**), the LS state is inherent to the 4d-metal centre.

Table 3. Susceptometric data for powders of complexes **1**–**7a**.

Compound	T/K	$\chi_m/10^{-3}$ cm^3 · mol^{-1}	μ_{eff}[a]	S[b]
1 · ½ H_2O	295.5(1)	13.0(4)	5.61(9)	2½ (HS)
2a · 2 H_2O[c]	295.5(1)	10.3(8)	5.0(2)	2 (HS)
2b[c]	296.3(1)	13.8(2)	5.75(4)	2½ (HS)
2c · 1½ H_2O · ½ MeOH[c]	296.0(1)	0.01(3)	0.83(4)	0 (LS)
3	295.3(1)	8.1(2)	4.47(5)	1½ (HS)
4 · H_2O	295.7(1)	4.1(2)	3.22(7)	1
5a · H_2O · MeOH	295.4(1)	1.39(4)	2.01(2)	½
6 · MeOH	298.0(1)	0.01(3)	0.85(4)	0
7a · ¾ PhMe	297.6(1)	0.08(4)	1.00(4)	0 (LS)

[a] Molar susceptibilities have been corrected for diamagnetic contributions to yield paramagnetic susceptibilities χ_P and effective magnetic moments $\mu_{eff} = (8\ \text{mol} \cdot \text{cm}^{-3} \cdot \text{K}^{-1} \cdot \chi_P T)^{½}$. [b] Estimation using a spin-only model: $\mu_{eff} \approx 2[S(S+1)]^{½}$. [c] Data have been published before and are included for comparison.[3b, 5]

Evaluated distortion parameters are listed in Table 4, along with data for the high-spin complex $[Fe^{III}Cl_2L]PF_6$ (**2b**) and the low-spin complex $[Fe^{II}(CN)_2L]$ (**2c**). The ordering of rows is by increasing effective ionic radius. Uncertainties of Ξ and Δr have been estimated on the basis of distance/angle standard-uncertainties from SHELXL-97 geometry calculations.[10]

Table 4. Distortion parameters and effective ionic radii[8] r_{eff} for complexes **1**–**6**.

	r_{eff}/Å	Δr/Å	Σ/°	$S(O_h)$	Ξ/°	Φ/°
2c[a]	0.61	0.06(3)	48.5(3)	0.66	10.0(6)	4.2(10)
2b[a]	0.645	0.17(3)	84.5(3)	1.66	21.2(6)	9.4(9)
5a[b]	0.65	0.15(3)	90.8(10)	5.13	22.7(9)	26.2(12)
4	0.690	0.08(2)	71.3(2)	1.77	16.3(6)	6.5(6)
6	0.740	0.17(3)	93.1(3)	2.19	22.0(9)	11.3(10)
3	0.745	0.12(4)	83.2(3)	2.04	20.5(6)	12.3(12)
2a[a]	0.780	0.16(3)	98.8(2)	2.47	18.7(6)	11.4(9)
1	0.830	0.24(2)	110.5(2)	2.74	60.2(6)	42.2(6)

[a] Data have been published before and are included for comparison.[3b, 5] [b] Data have been calculated with the non-coordinating chloride ion as sixth vertex of an octahedron.

The centre displacement Δr and tetragonal distortion Σ do not show any clear trend with regard to the ionic radii. They are, however, minimal/maximal for the LS-iron(II)/HS-manganese(II) complex **2c**/**1**, being the complex with the smallest/largest central ion in the sample, respectively. Excluding these extrema, all values lie around $\Delta r \approx 0.14$ Å and $\Sigma \approx 87°$. The behaviour of these parameters cannot be described by the size of the metal ion alone, being probably also subject to electronic effects, other geometric restraints than have been taken into account, or packing effects. This is contrary to the findings for the CSM $S(O_h)$ (see Fig. 4).

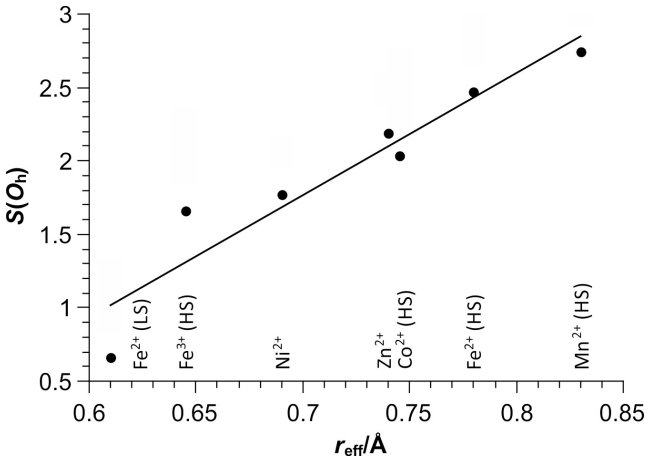

Figure 4. Plot[11] of the CSM for the deviation from an octahedron against the effective ionic radius.

The data points suggest a roughly linear increase of $S(O_h)$ with r_{eff}. Regression analysis indeed allows for a linear fit following Eq. 3 with an acceptable coefficient of determination ($R^2 = 0.9247$). This means that, in the range considered, the overall distortion of the coordination octahedron may be explained by the sterical demand of the central ion alone.

$$S(O_h) = 8.3(12)\ \text{Å}^{-1} \cdot r_{eff} - 4.1(9) \quad (3)$$

Extrapolation to $S(O_h) = 0$ leads to an estimate of $r_{eff} \approx 0.5$ Å as ideal for minimal distortion. (A CSM value of zero cannot be reached in reality, as this would require all metal-donor bonds to be of equal length.) Candidates with ionic radii of 0.45–0.55 Å in octahedral coordination and with good synthetic accessibility are Al^{3+}, LS-Co^{3+}, LS-Fe^{3+} and Ge^{4+}, probably making a change of monodentate ligands necessary. The linear model is, however, to be understood as purely empirical-phenomenological.

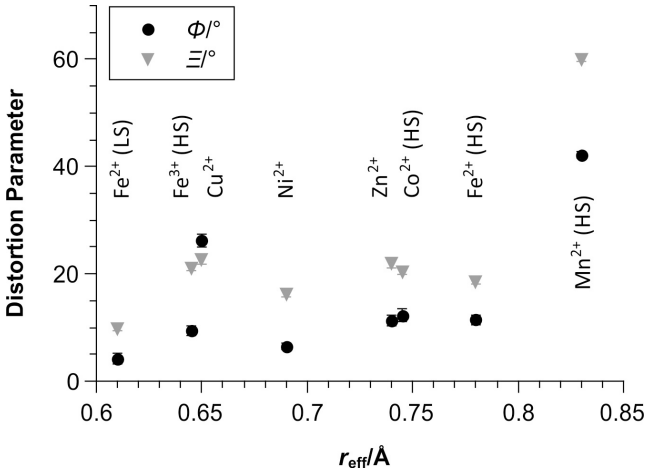

Figure 5. Plot[11] of the ligand-distortion parameters against the effective ionic radius.

Ring tilt and ring twist as parameters of ligand distortion behave quite similarly to Δr and Σ (see Fig. 5). They show extremal values for **2c** and **1**, but do not indicate a clear

trend in between, averaging to $\Xi \approx 20°$ and $\Phi \approx 10°$. Additionally, their characteristics are similar, except for one feature: The ring twist Φ is disproportionately high in the copper(II) complex **5a**. This fact is due to a large twist angle for the pyridyl residue containing N30, being part of the axis of Jahn-Teller distortion. The ligand deformation may not adequately be described as a function of the ionic radius alone. Other subtle effects (see above) seem to play an equally important role.

Oxidation Stability of [$Mn^{II}Cl_2L$] (1)

Apart from these considerations of molecular structure, we observed remarkable reactivity in some of the complexes. The manganese(II) complex **1** stands out due to its inertness towards oxidation, even though manganese(III) complexes are numerous and, if coordinated by electron-rich ligands, often more stable than their low-valent analogues. In contrast to this, [$Mn^{II}Cl_2L$] (**1**) cannot be oxidised to a manganese(III) complex by dioxygen, hydrogen peroxide or iodosylbenzene. When a light yellow solution of **1** in methanol/water is reacted with one of the latter oxidants, flakes of manganese(IV) oxide precipitate without any colour change of the solution, as would be characteristic for the formation of manganese(III). The reaction is sluggish, so that it may take more than 24 h to subside.

In other contexts, the failure of attempts to synthesise dicyanidoiron(III) and dicarbonyliron(II) complexes of L has already hinted at the ligand being a relatively weak donor, but good π-acceptor. This is in line with the stabilisation of lower (electron-richer) oxidation states, such as manganese(II). Further experiments with structurally related tris(pyridyl)ethane-derived ligands have shown that oxidation to manganese(III) is only possible if activated (picolinic) protons are in contact with the inner coordination sphere, and an alcoholic solvent is present. Under these circumstances, dioxygen or hydrogen peroxide oxidise the ligand, thereby forming a pentadentate chelator containing a strong alkoxido donor. The O donor then substitutes a chlorido ligand, which creates a coordination sphere sufficiently electron-rich for the oxidation of the central ion to proceed, finally yielding a deep red manganese(III) complex.[12]

Complexes of Heavier Group 8 Metals

In addition to complexes of L with 3d metals, ruthenium(II) compounds—as representatives of heavier homologues—are also accessible. They can be synthesised by ligand exchange at the coordinatively unsaturated, 16 valence-electron complex [$Ru^{II}Cl_2(PPh_3)_3$] (see Scheme 2). Because of the inertness of this precursor, the reaction requires elevated temperature (boiling toluene).

While the precursor is sensitive towards dioxygen, the reaction product **7a** is air-stable in solution for several days. (This effect is probably due to effective shielding of the metal centre by the chelator L.) Although no single crystals of **7a** could be obtained, we assigned it the same constitution as the 3d-metal complexes—in accordance with analytical data (see Experimental Section), structures of derivatives and the lack of additional suitable ligands. X-ray structure-determination was performed on two pseudopolymorphs of [RuClL(MeCN)]Cl that crystallised from wet acetonitrile solutions of **7a** via isothermal diffusion of diethyl-ether vapour. Owing to severe disorder problems, however, the analyses only yielded models of very poor quality.[13] We overcame this problem by exchanging the chloride for an iodide counter-ion using tetrabutylammonium iodide (see Scheme 2). The resulting compound [Ru^{II}ClL(MeCN)]I (**7b**) readily crystallised in the monoclinic space group $P2_1/c$ with one complex cation in the asymmetric unit (see Fig. 6). Structural and spectroscopic analyses do not hint at substitution of the chlorido by an iodido ligand. Compound **7b** as well as the pseudopolymorphs of [RuClL(MeCN)]Cl show one striking difference to the 3d-metal complexes: the exchange of a chlorido against an acetonitrile ligand. This is due to the softer ruthenium(II) ion being more efficiently stabilised by soft π-acceptors than by hard σ-donors.

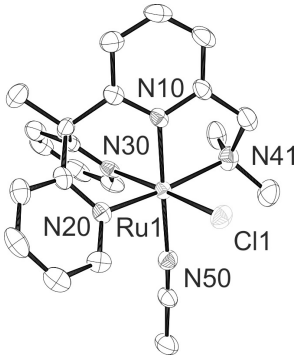

Figure 6. ORTEP plot of **7b**. Ellipsoids for 50 % probability, hydrogen atoms and iodide counter-ion omitted for clarity. Selected bond lengths *d*/Å: N10–Ru1 1.997(4), N20–Ru1 2.032(4), N30–Ru1 2.049(4), N41–Ru1 2.191(5), N50–Ru1 2.050(5), Cl1–Ru1 2.4393(13).

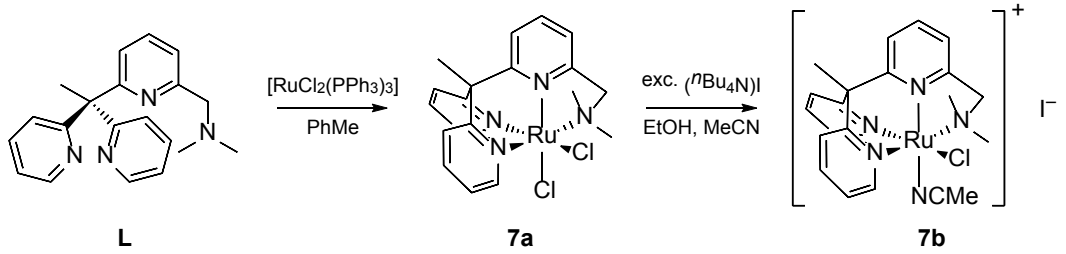

Scheme 2. Synthesis of the ruthenium(II) complexes **7a** and **7b**.

In the crystal, each of the molecules of **7b** forms two π stacks with symmetry-equivalent rings of neighbouring complexes, leading to infinite zigzag chains along [100]. The counter ions occupy lipophilic pockets, forming two short contacts to methyl groups and one to a ring hydrogen-atom. This arrangement, which mirrors the softness of the iodide ions, accounts for the absence of hydrogen-bonding solvent molecules from the structure and the high degree of order compared to the chloride derivative.

Further, a feature in the ESI mass-spectrum of $[Ru^{II}Cl_2L]$ (**7a**) is worth noting (see Fig. 7): Besides the expected signal of $[Ru^{II}ClL]^+$ (m/z = 455.0565), one for the dinitrogen complex $[Ru^{II}ClL(N_2)]^+$ (m/z = 483.0631) is recorded with high intensity. Elemental analysis clarifies that this species forms in the ion source of the spectrometer and is not present in the substance itself. However, its occurrence corroborates that one of the chlorido ligands in **7a** is labile towards substitution by π acceptors, thus enabling the coordination of small molecules to the ruthenium(II) centre.

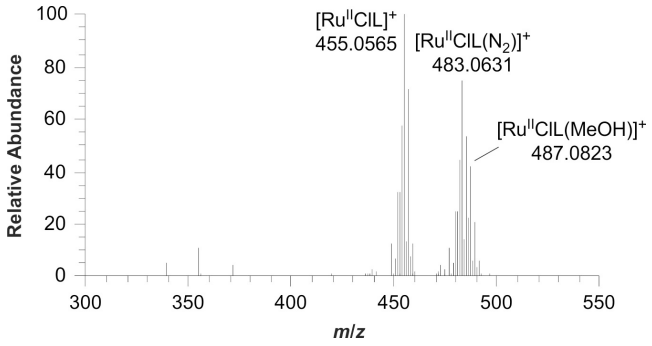

Figure 7. Detail of the ESI(+) mass-spectrum of **7a** in methanol.

We were unable to synthesise the osmium analogue of **2a**/**7a**, $[Os^{II}Cl_2L]$. In our hands, attempts to exchange ligands at $[Os^{II}Cl_2(PPh_3)_3]$[14] in boiling toluene failed, yielding greenish to brown mixtures that are heterogeneous (according to elemental analyses), paramagnetic and contain phosphanes (according to NMR spectroscopy). Apparently, L is unfit properly to stabilise and shield the large and very soft osmium(II) ion. Intermediary complexes may thus be prone to incomplete substitution of the soft triphenylphosphane ligands with the harder N_4 chelator L, and be especially sensitive towards oxidation.

Conclusions

In 3d-metal(II) complexes of L, the distortion of the ligand, and hence the coordination polyhedron, does not dependent on the size of the metal ion in a uniform fashion. Whereas all examined distortion parameters are minimal for LS-iron(II) and maximal for HS-manganese(II), only the CSM $S(O_h)$—quantifying the total deviation of the coordination geometry from an ideal octahedron—is a function solely of the effective ionic radii (namely, a linear one). Other indicators of deformation primarily incorporating bond lengths (centre displacement Δr) or bond angles (tetragonal distortion Σ) do not exhibit such a correlation. The same holds for the ligand-distortion parameters, ring tilt Ξ and ring twist Φ, introduced herein. We conclude that the overall distortion of the coordination environment is predominantly determined by the steric demand of the central ion, while electronic or other more subtle influences essentially contribute to the deformation of the ligand L.

Although L is flexible enough to accommodate larger 3d- and even 4d-metal(II) ions in a stable manner, it offers an environment ideal for small metal ions (estimate: 0.4–0.6 Å), such as LS-iron(II) with r_{eff} = 0.61 Å. This is most likely the reason for the "delayed" thermal SCO observed in the complex $[Fe^{II}L(NCS)_2]$ (**2d**): The ligand stabilises/destabilises the LS/HS state, respectively, leading to a higher transition enthalpy und thus a higher transition temperature.

The surprising stability of $[Mn^{II}Cl_2L]$ (**1**) against dioxygen and other strong oxidants can be attributed, on the one hand, to its electron deficiency, and to the absence of activated hydrogen atoms near the first coordination sphere on the other. This prevents metal-mediated activation and possibly opens a route towards catalysts for the oxidation of aliphatic methine groups with hydrogen peroxide (as reported for structurally related amine-pyridine donors).[15]

As evidenced by solution reactivity and mass spectrometry, $[Ru^{II}Cl_2L]$ (**7a**) is capable of exchanging one chlorido ligand against small π-accepting molecules such as acetonitrile and dinitrogen. Attempts to isolate complexes of the latter and similar ligands targeting activation of small molecules are in progress. Although an osmium(II) complex of L was inaccessible, it can possibly be prepared using a set of softer donors, e.g., a substituted phosphanyl or sulfanyl instead of the dimethylamino group. As well as ruthenium(II), osmium(II) compounds may also be of interest as possible photosensitisers on metal oxides for photovoltaics applications.[16]

Table 1. Crystallographic data and structure refinement details.

	1	**3** · ½ MeOH	**4** · ½ MeOH	**5** · ½ Et_2O · MeOH	**6** · ½ MeOH	**7b**
CCDC No.	983974	983975	983976	983977	983978	983979
Empirical formula	$C_{20}H_{22}Cl_2MnN_4$	$C_{20.5}H_{24}Cl_2CoN_4O_{0.5}$	$C_{20.5}H_{24}Cl_2N_4NiO_{0.5}$	$C_{23}H_{31}Cl_2CuN_4O_{1.5}$	$C_{20.5}H_{24}Cl_2N_4O_{0.5}Zn$	$C_{22}H_{25}ClIN_5Ru$
M/g · mol^{-1}	444.26	464.27	464.05	521.96	470.71	622.89
Crystal system	monoclinic	monoclinic	monoclinic	monoclinic	monoclinic	monoclinic
Space group	$P2_1/c$ (No. 14)	$P2_1/c$ (No. 14)	$P2_1/c$ (No. 14)	$C2/c$ (No. 15)	$P2_1/c$ (No. 14)	$P2_1/c$ (No. 14)
a/Å	9.4818(6)	11.1848(4)	9.2724(6)	24.854(3)	11.2065(9)	12.0428(3)
b/Å	14.2261(9)	9.9247(5)	15.8029(7)	13.0944(15)	9.9892(8)	11.1038(3)
c/Å	16.4749(12)	18.7364(8)	14.4519(9)	14.7180(14)	18.6169(16)	17.2738(8)
α/°	90	90	90	90	90	90
β/°	115.120(5)	93.368(4)	100.329(7)	96.440(9)	92.834(8)	95.203(3)
γ/°	90	90	90	90	90	90
V/Å^3	2012.1(2)	2076.26(16)	2083.3(2)	4759.7(9)	2081.5(3)	2300.35(14)
Z	4	4	4	8	4	4
ρ_{calc}/g · cm^{-3}	1.467	1.485	1.479	1.457	1.502	1.799
Crystal description	pale yellow column	dark violet prism	light blue octahedron	dark blue shard	colourless prism	light red shard
Crystal dimensions/ mm^3	0.07 × 0.07 × 0.15	0.21 × 0.16 × 0.15	0.28 × 0.24 × 0.23	0.15 × 0.12 × 0.05	0.22 × 0.18 × 0.13	0.28 × 0.14 × 0.12
μ/mm^{-1}	0.934	1.100	1.204	1.168	1.453	2.159
T(min, max)	0.83394/1.0000	0.88457/1.0000	0.90665/1.0000	0.81548/1.0000	0.61910/1.0000	0.55067/1.0000
θ(min, max)/°	3.51/25.00	3.44/26.00	3.41/26.00	3.36/26.00	3.45/26.00	3.34/26.00
Miller indices	$-11 \le h \le 11$, $-16 \le k \le 16$, $-16 \le l \le 19$	$-9 \le h \le 13$, $-11 \le k \le 12$, $-23 \le l \le 22$	$-7 \le h \le 11$, $-16 \le k \le 19$, $-17 \le l \le 17$	$-30 \le h \le 30$, $-16 \le k \le 16$, $-18 \le l \le 18$	$-6 \le h \le 13$, $-9 \le k \le 12$, $-21 \le l \le 22$	$-14 \le h \le 14$, $-8 \le k \le 13$, $-18 \le l \le 21$
Reflections	14655	9712	9247	18326	9371	17122
independent (R_{int})	3532 (0.0299)	4073 (0.0239)	4086 (0.0171)	4673 (0.0674)	4080 (0.0364)	4513 (0.0415)
observed[a] (R_σ)	2952 (0.0295)	3336 (0.0337)	3475 (0.0245)	3895 (0.0625)	3628 (0.0421)	3894 (0.0423)
Data, restr., param.	3532/0/247	4073/0/267	4086/0/248	4673/0/268	4080/13/267	4513/0/276
R_1/wR_2[b] (all)	0.0400/0.0723	0.0545/0.0997	0.0337/0.0806	0.0671/0.1197	0.0441/0.0898	0.0631/0.1077
R_1/wR_2[b] (observed)	0.0288/0.0699	0.0411/0.0955	0.0270/0.0789	0.0510/0.1128	0.0366/0.867	0.0511/0.1026
u, v[b]	0.0432/0.0000	0.0465/2.4742	0.0527/0.1948	0.0516/7.3776	0.0368/2.2149	0.0402/3.9272
S, S'	1.061/1.061	1.028/1.028	1.028/1.028	1.099/1.099	1.028/1.028	1.161/1.161
ρ_e(min, max)/e · Å^{-3}	–0.237/0.348	–0.445/1.133	–0.274/0.334	–0.467/0.444	–0.550/0.681	–0.771/1.239

[a] $I > 2\sigma(I)$. [b] $R_1 = \Sigma||F_o| - |F_c||/\Sigma|F_o|$, $wR_2 = [\Sigma w(F_o^2 - F_c^2)^2/\Sigma wF_o^4]^{½}$, $w = [\sigma^2(F_o^2) + (uP)^2 + vP]^{-1}$ mit $P = [\max(F_o^2, 0) + 2F_c^2]/3$.

Experimental Section

Materials and General Methods: $[RuCl_2(PPh_3)_3]$[17] and ligand L[3] were prepared according to published procedures. All other chemicals were purchased from Sigma-Aldrich or Acros Organics and used without further purification. Air- or moisture-sensitive compounds were handled in dry solvents under dry dinitrogen, using standard Schlenk techniques. Where noted, solvents were degassed applying three freeze-pump-thaw cycles.

Analytical Methods: *NMR spectra* were recorded on a "Bruker ARX 200" at r.t. Chemical shifts refer to $SiMe_4$ and have been calibrated with respect to the residual proton signal for ^1H ([D$_5$]DMSO: $\delta = 2.50$ ppm, $CHCl_3$: $\delta = 7.26$ ppm) or the solvent signal for ^{13}C ([D$_6$]DMSO: $\delta = 39.52$ ppm).[18] *IR spectra* in attenuated total reflectance (ATR) were measured with a "Thermo Nicolet iS5" equipped with a "Thermo Nicolet iD5" ZnSe sample-holder, those of CsCl pellets with a "Nicolet Magna System 750". *Mass spectra* were recorded in ESI(+) mode with a "Thermo Scientific Orbitrap LTQ XL" (spray voltage: 5 kV, source temperature: 275 °C). *UV/Vis spectra* were obtained using a "Varian Cary 50" spectrophotometer. *Elemental analyses* were performed using "Thermo Finnigan EAGER 300" and "elementar vario EL" devices. *Susceptometry* was carried out at r.t. using a "Johnson Matthey MSB Auto" magnetic balance calibrated with tridistilled water ($\chi_g = -7.2 \cdot 10^{-7}$ cm^3 · g^{-1}). The susceptibility of L measured in MeOH was $\chi_D = -2.07 \cdot 10^{-4}$ cm^3 · mol^{-1}; further diamagnetic contributions were corrected for using Pascal's constants.[19]

X-Ray Crystallography: Data were collected at 150.00(10) K using an "Oxford Diffraction Xcalibur S" diffractometer equipped with a goniometer in κ geometry, a "Sapphire 3" CCD-detector, and a graphite-monochromated "Enhance" Mo-K_α source ($\lambda = 0.71073$ Å). Diffraction images were integrated with CrysAlisPro. An empirical absorption correction using spherical harmonics implemented in the Scale3 AbsPack scaling algorithm was performed.[20] Structures were solved with Superflip[21] (**7b**) or ShelXS-97[10] using direct methods (all others) and refined with ShelXL-97[10] against F_o^2 data using the full-matrix least-squares algorithm. Non-hydrogen atoms were refined anisotropically; hydrogen atoms were refined isotropically with standard riding-models. The methanol moiety in **3** is disordered over a centre of inversion and was modelled in two discrete positions with halved occupation. The methanol moiety in **4** and the diethyl-ether moiety

in **5a** could be detected but not refined satisfactorily. They were subsequently treated as a diffuse contribution to the overall scattering without specific atom positions with SQUEEZE/PLATON.[22] Molecular graphics were produced using ORTEP-3 FOR WINDOWS.[23] Continuous symmetry measures (CSM) were calculated using the internet service of the Hebrew University of Jerusalem.[24] All other parameters were derived from SHELXL-97 output using basic arithmetic or statistical methods.

Synthesis of 3d-Metal Complexes 1 and 3–6: A solution of L (1.1 eq) in methanol (1.5 mL) was added dropwise to a solution of the (hydrated) metal(II) chloride (1.0 eq) in methanol (1.5 mL) while stirring at r.t. The mixture was stirred for a further 30 min. The complex was exhaustively precipitated and washed with MTBE (3 × 30 mL). After 12 h in medium vacuum, solvated complexes **1** and **3**–**6** remained as coloured powders (see Table 5).
Crystals suitable for X-ray structure-determination were obtained by vapour diffusion of diethyl ether into wet methanolic solutions of the complexes during one week at r.t.

[$MnCl_2$L] (1): ^{1}**H NMR** (200 MHz, [D_6]DMSO): δ = 8.46, 7.62, 7.19, 6.94, 6.80 ppm (all br m). **IR** (CsCl): $\tilde{\nu}$ = 3086, 3005, 2985, 2958, 2924, 2875 (m, ν[CH]), 1596, 1588, 1576 (vs, ν[C=N], ν[C=C]), 1480, 1437, 1389 (vs, δ[CH]), 1303 (w), 1292, 1254 (m), 1201 (w), 1164, 1105, 1081, 833, 798, 781, 767 (m, γ[CH]), 635 (m, δ[C=C], δ[C=N]), 420 (m, γ[C=C], γ[C=N]), 232 cm^{-1} (m, ν[MnCl]). **UV/Vis** (MeOH): λ_{max} (ε) = 324 (760), 263 (18200), 207 nm (26200 cm^2 · mmol^{-1}). **MS** (ESI+, MeOH): *m*/*z* = 186.56 ([M – 2Cl]$^{2+}$, 3), 319.19 ([L + H]$^+$, 100), 408.09 ([M – Cl]$^+$, 3), 762.25 ([M + L + H]$^+$, 2 %). **Anal.** for $C_{20}H_{22}Cl_2MnN_4 \cdot ½\ H_2O$ (453.26): C 52.96 (calcd. 53.00), H 5.06 (5.11), N 12.34 (12.36) %.

[$CoCl_2$L] (3): ^{1}**H NMR** (200 MHz, [D_6]DMSO): δ = 99.29, 74.29, 55.46, 43.83, 28.62 ppm (all br m). **IR** (CsCl): $\tilde{\nu}$ = 3071, 2968, 2890, 2784 (m, ν[CH]), 1593, 1579 (vs, ν[C=N], ν[C=C]), 1480, 1437, 1383, 1370 (vs, δ[CH]), 1309, 1294, 1253, 1201 (w), 1166, 790, 771, 759, 748, 710 (m, γ[CH]), 629 (m, δ[C=C], δ[C=N]), 431 (m, γ[C=C], γ[C=N]), 226 cm^{-1} (m, ν[CoCl]). **UV/Vis** (MeOH): λ_{max} (ε) = 608 (10), 545 (20), 524 (20), 503 (20), 462 (20), 263 (14000), 207 nm (28600 cm^2 · mmol^{-1}). **MS** (ESI+, MeOH): *m*/*z* = 412.09 ([M – Cl]$^+$, 100 %). **Anal.** for $C_{20}H_{22}CoCl_2N_4$ (448.25): C 53.70 (calcd. 53.59), H 5.11 (4.95), N 12.49 (12.50) %.

[$NiCl_2$L] (4): ^{1}**H NMR** (200 MHz, [D_6]DMSO): δ = 61.74, 55.46, 55.24, 43.83, 16.72, 15.36, 11.18 ppm (all br m). **IR** (CsCl): $\tilde{\nu}$ = 3105, 3074, 2959, 2889 (m, ν[CH]), 1594, 1579 (vs, ν[C=N], ν[C=C]), 1480, 1438, 1383 (vs, δ[CH]), 1294 (m), 1295 (w), 1166 (s), 790, 772, 750, 712 (m, γ[CH]), 639 (m, δ[C=C], δ[C=N]), 436 (m, γ[C=C], γ[C=N]), 281, 267 (m, ν[NiCl]), 237 cm^{-1} (m, ν[NiN]). **UV/Vis** (MeOH): λ_{max} (ε) = 967 (30), 804 (10), 664 (6), 570 (10), 264 (10500), 206 nm (26500 cm^2 · mmol^{-1}). **MS** (ESI+, MeOH): *m*/*z* = 411.09 ([M – Cl]$^+$, 34), 188.06 ([M – 2Cl]$^{2+}$, 48 %). **Anal.** for $C_{20}H_{22}Cl_2N_4Ni \cdot H_2O$ (466.03): C 51.50 (calcd. 51.54), H 5.05 (5.19), N 11.91 (12.02) %.

[CuClL]Cl (5a): ^{1}**H NMR** (200 MHz, [D_6]DMSO): δ = 13.26, 7.41 ppm (all br m). **IR** (CsCl): $\tilde{\nu}$ = 3107, 3076, 3061, 3016, 2978, 2908 (s, ν[CH]), 1593, 1579 (vs, ν[C=N], ν[C=C]), 1480, 1442, 1386 (vs, δ[CH]), 1311 (w) , 1297 (m), 1271 (w), 1207, 1230, 1179 (m), 1167 (s), 1155 (w), 805, 784, 775 (m), 760 (w), 715 (m, γ[CH]), 641 (m, δ[C=C], δ[C=N]), 476 (m, γ[C=C], γ[C=N]), 366, 336, 272, 266 (m, ν[CuN]), 247 (m), 221 cm^{-1} (m, ν[CuCl]). **UV/Vis** (MeOH): λ_{max} (ε) = 720 (140), 639 (140), 264 nm (18100 cm^2 · mmol^{-1}). **MS** (ESI+, MeOH): *m*/*z* = 416.08 ([M]$^+$, 56), 412.13 ([M – Cl + OMe]$^+$, 100), 319.19 ([L + H]$^+$, 23), 190.56 ([M – Cl]$^{2+}$), 45 %). **Anal.** for $C_{20}H_{22}Cl_2CuN_4 \cdot H_2O \cdot CH_4O$ (502.92): C 50.56 (calcd. 50.15), H 5.47 (5.61), N 11.28 (11.14) %.

[$ZnCl_2$L] (6): ^{1}**H NMR** (200 MHz, [D_6]DMSO):[25] δ = 8.67 (br m, 2 H, 6′H, 6″H), 7.81 (br m, 4 H, aryl H),[26] 7.34 (br m, 4 H, aryl H), 3.71 (br m, 2 H, CH_2), 2.34 (s, 3 H, C–CH_3), 2.19 ppm (s, 6 H, N–CH_3). ^{13}**C{^{1}H} NMR** (100 MHz, [D_6]DMSO): δ = 161.9 (br, 2′C, 2″C, 6C), 156.2 (2C), 149.8 (6′C, 6″C), 140.1 (br, 4C), 138.8 (br, 4′C, 4″C), 123.2 (3′C, 3″C), 122.9 (3C, 5C), 122.3 (5′C, 5″C), 62.6 (br, CH_2), 45.3 (N–CH_3), 26.2 ppm (C–CH_3). **IR** (CsCl): $\tilde{\nu}$ = 3084, 3064, 2964, 2879, 2844, 2788 (m, ν[CH]), 1597, 1586, 1578 (m, ν[C=N], ν[C=C]), 1480, 1439, 1389 (vs, δ[CH]), 1365 (m), 1303 (w), 1288, 1256, 1221 (m), 1203 (w), 798, 782, 767, 710 (m, γ[CH]), 636 (m, δ[C=C], δ[C=N]), 424 (m, γ[C=C], γ[C=N]), 280, 259 cm^{-1} (m, ν[ZnCl]). **UV/Vis** (MeOH): λ_{max} (ε) = 263 (12900), 204 nm (18200 cm^2 · mmol^{-1}). **MS** (ESI+, MeOH): *m*/*z* = 417.08 ([M – Cl]$^+$, 100), 319.19 ([L + H]$^+$, 43), 191.06 ([M – 2Cl]$^{2+}$, 80 %). **Anal.** for $C_{20}H_{22}Cl_2N_4Zn \cdot CH_4O$ (486.74): C 52.03 (calcd. 51.82), H 5.32 (5.38), N 11.49 (11.51) %.

Synthesis of [$RuCl_2$L] (7a): [$RuCl_2(PPh_3)_3$] (633 mg, 0.66 mmol) was added to a solution of L (232 mg, 0.73 mmol) in degassed toluene (40 mL) under exclusion of air. The resulting brown solution was refluxed for 1 h. During this time, a cherry-red precipitate formed. After cooling to r.t., the light orange-red suspension was filtered. The remaining solid was washed with degassed toluene (3 × 5 mL) and diethyl ether (3 × 5 mL). Evaporation of solvent residues in medium vacuum yielded [$RuCl_2$L] (**7a**) · ¾ PhMe (337 mg, 91 %) as a red powder. ^{1}**H NMR** (200 MHz, $CDCl_3$): δ = 8.45 (br m, 1 H), 8.18 (br m, 2 H), 8.02 (m, 1 H), 7.72 (m, 3 H), 7.56 (m, 1 H), 7.38 (d, $^3J_{HH}$ = 7.0 Hz, 1 H), 7.19–7.12 (m, 5 H, *Ph*–Me), 6.80 (d, $^3J_{HH}$ = 7.0 Hz, 1 H), 6.04 (br m, 1 H), 3.37 (br s, 1 H, CH_2), 2.87 (br s, 3 H, N–CH_3), 2.75 (s, 3 H, C–CH_3), 2.32 (s, 3 H, Ph–*Me*), 1.69 (br s, 1 H, CH_2), 1.19 ppm (br s, 3 H, N–CH_3). **IR** (ATR): $\tilde{\nu}$ = 3096, 3059, 3016, 2978, 2892, 2854, 2785 (w, ν[CH]), 1638, 1600, 1555 (w, ν[C=N], ν[C=C]), 1457, 1429, 1404 (s, δ[CH]), 1385, 1354, 1302, 1237 (w), 1170, 1149 (m), 1109, 1080, 1052, 1026, 1014, 995, 983, 966 (w), 853, 844 (m), 764, 738 (s, γ[CH]), 715, 699, 655, 648, 612 cm^{-1} (m, δ[C=C], δ[C=N]). **UV/Vis** (MeOH): λ_{max} (ε) = 435 (10100), 388 nm (11500 cm^2 · mmol^{-1}). **MS** (ESI+, MeOH): *m*/*z* = 487.08 ([M – Cl + MeOH]$^+$, 42), 483.06 ([M – Cl + N_2]$^+$, 75), 455.06 ([M – Cl]$^+$, 100 %). **Anal.** for $C_{20}H_{22}Cl_2N_4Ru \cdot ¾\ C_7H_8$ (559.50): C 54.21 (calcd. 54.20), H 4.93 (5.04), N 9.82 (10.01) %.

Synthesis of [RuClL(MeCN)]I (7b): [$RuCl_2$L] (**7a**) · ¾ PhMe and an excess of ($n$$Bu_4$N)I were briefly heated in ethanol. The resulting orange-red precipitate was recrystallised by vapour diffusion of diethyl ether into a solution in acetonitrile during four weeks at r.t. Crystals were suitable for X-ray structure-determination.

Table 5. Synthesis and description of 3d-metal complexes **1** and **3**–**6**.

Metal(II) chloride		Ligand L	Product	Yield	Colour
$MnCl_2 \cdot 4\ H_2O$	(73 mg, 0.37 mmol)	129 mg, 0.41 mmol	$[MnCl_2L]$ (**1**) $\cdot$ ½ H_2O	155 mg, 92 %	light yellow
$CoCl_2 \cdot 6\ H_2O$	(86 mg, 0.36 mmol)	127 mg, 0.40 mmol	$[CoCl_2L]$ (**3**)	157 mg, 97 %	violet
$NiCl_2 \cdot 6\ H_2O$	(88 mg, 0.37 mmol)	129 mg, 0.41 mmol	$[NiCl_2L]$ (**4**) $\cdot$ H_2O	139 mg, 81 %	light blue
$CuCl_2 \cdot 2\ H_2O$	(68 mg, 0.40 mmol)	140 mg, 0.44 mmol	[CuClL]Cl (**5**) $\cdot$ H_2O $\cdot$ MeOH	151 mg, 75 %	dark blue
$ZnCl_2$	(49 mg, 0.36 mmol)	126 mg, 0.40 mmol	$[ZnCl_2L]$ (**6**) $\cdot$ MeOH	137 mg, 78 %	colourless

Acknowledgement

Financial support by the Deutsche Forschungsgemeinschaft (SFB 658: Elementary Processes in Molecular Switches on Surfaces) is gratefully acknowledged. We thank Marek Sokolowski, B.Sc. for practical assistance with syntheses and spectroscopic characterisation.

[1] J. A. McCleverty, T. J. Meyer (Eds.), *Comprehensive Coordination Chemistry II: From Biology to Nanotechnology*, Elsevier, Amsterdam, **2003**.

[2] A. Grohmann, *Dalton Trans.* **2010**, *39*, 1432–1440.

[3] a) E. A. Ünal, D. Wiedemann, J. Seiffert, J. P. Boyd, A. Grohmann, *Tetrahedron Lett.* **2012**, *53*, 54–55; b) D. Wiedemann, E. Świętek, W. Macyk, A. Grohmann, *Z. Anorg. Allg. Chem.* **2013**, *649*, 1483–1490.

[4] M. Bernien, D. Wiedemann, C. F. Hermanns, A. Krüger, D. Rolf, W. Kroener, P. Müller, A. Grohmann, W. Kuch, *J. Phys. Chem. Lett.* **2012**, *3*, 3431–3434.

[5] D. Wiedemann, A. Grohmann, *Dalton Trans.* **2014**, *43*, 2406–2417.

[6] H. Zabrodsky, S. Peleg, D. Avnir, *J. Am. Chem. Soc.* **1992**, *114*, 7843–7851.

[7] P. Guionneau, C. Brigouleix, Y. Barrans, A. E. Goeta, J.-F. Létard, J. A. K. Howard, J. Gaultier, D. Chasseau, *C. R. Acad. Sci., Ser. IIc: Chim.* **2001**, *4*, 161–171.

[8] R. Shannon, *Acta Crystallogr., Sect. A: Found. Crystallogr.* **1976**, *32*, 751–767.

[9] L. N. Mulay, *Magnetic Susceptibility*, John Wiley, New York, **1963**.

[10] G. M. Sheldrick, *Acta Crystallogr., Sect. A: Found. Crystallogr.* **2008**, *64*, 112–122.

[11] I. Vasilef, QTIPLOT, Data Analysis and Scientific Visualisation, Universiteit Utrecht, Utrecht, Netherlands, **2013**.

[12] K. Student, *Dissertation*, Technische Universität Berlin, **2013**.

[13] $[RuClL(MeCN)]Cl \cdot H_2O$: a = 9.6783(4) Å, b = 12.7017(8) Å, c = 19.2168(9) Å, α = 90°, β = 90°, γ = 90°, Z = 4, *Pnma*, disorder of complexes about a mirror plane. $[RuClL(MeCN)]Cl \cdot 1½\ Et_2O$: a = 8.1605(13) Å, b = 12.799(2) Å, c = 13.485(2) Å, α = 72.338(15)°, β = 85.041(12)°, γ = 76.532(15)°, Z = 2, $P\bar{1}$, unresolvable disorder of diethyl-ether molecules.

[14] S. Bhattacharya, C. G. Pierpont, *Inorg. Chem.* **1991**, *30*, 2906–2911.

[15] R. V. Ottenbacher, D. G. Samsonenko, E. P. Talsi, K. P. Bryliakov, *Org. Lett.* **2012**, *14*, 4310–4313.

[16] A. Hagfeldt, G. Boschloo, L. Sun, L. Kloo, H. Pettersson, *Chem. Rev.* **2010**, *110*, 6595–6663.

[17] P. S. Hallman, T. A. Stephenson, G. Wilkinson, in *Inorganic Syntheses, Vol. 12* (Ed.: R. W. Parry), McGraw-Hill, New York, **1970**, pp. 237–240.

[18] G. R. Fulmer, A. J. M. Miller, N. H. Sherden, H. E. Gottlieb, A. Nudelman, B. M. Stoltz, J. E. Bercaw, K. I. Goldberg, *Organometallics* **2010**, *29*, 2176–2179.

[19] G. A. Bain, J. F. Berry, *J. Chem. Educ.* **2008**, *85*, 532–536.

[20] Agilent Technologies, CRYSALISPRO, Intelligent Data Collection and Processing Software for Small Molecule and Protein Crystallography, Agilent Technologies Ltd., Oxford, United Kingdom, **2013**.

[21] L. Palatinus, G. Chapuis, *J. Appl. Crystallogr.* **2007**, *40*, 786–790.

[22] P. van der Sluis, A. L. Spek, *Acta Crystallogr., Sect. A: Found. Crystallogr.* **1990**, *46*, 194–201.

[23] L. J. Farrugia, *J. Appl. Crystallogr.* **1997**, *30*, 565.

[24] A. Zayit, M. Pinsky, H. Elgavi, C. Dryzun, D. Avnir, *Chirality* **2011**, *23*, 17–23.

[25] The numbering scheme is given in Fig. 1. Single and double primed numbers refer to—through coordination—chemically inequivalent pyridyl residues in an arbitrary fashion.

[26] Due to their broadness and high multiplicity, the signals in the aromatic range could not be explicitly assigned to distinct proton types.

Received: January 29, 2014
Published online: April 3, 2014

Entry for the Table of Contents